Structural Basis for Substrate Specificity Differences of Horse Liver Alcohol Dehydrogenase Isozymes[†]

Hans-Werner Adolph,*[,‡] Peter Zwart,[§] Rob Meijers,[§] Ina Hubatsch,[‡,#] Martin Kiefer,[‡] Victor Lamzin,[§] and Eila Cedergren-Zeppezauer*[,||]

Fachrichtung 8.8 Biochemie, Universität des Saarlandes, D-66041 Saarbrücken, Federal Republic of Germany, EMBL, Hamburg Outstation, c/o DESY, Notkestrasse 85, D-22603 Hamburg, Federal Republic of Germany, Department of Biochemistry, Center for Chemistry and Chemical Engeneering, Lund University, P.O. Box 124, S-22100 Lund, Sweden

Received June 15, 2000

ABSTRACT: A structure determination in combination with a kinetic study of the steroid converting isozyme of horse liver alcohol dehydrogenase, SS-ADH, is presented. Kinetic parameters for the substrates, 5β-androstane-3β,17β-ol, 5β-androstane-17β-ol-3-one, ethanol, and various secondary alcohols and the corresponding ketones are compared for the SS- and EE-isozymes which differ by nine amino acid substitutions and one deletion. Differences in substrate specificity and stereoselectivity are explained on the basis of individual kinetic rate constants for the underlying ordered bi-bi mechanism. SS-ADH was crystallized in complex with 3α,7α,12α-trihydroxy-5β-cholan-24-acid (cholic acid) and NAD^+, but microspectrophotometric analysis of single crystals proved it to be a mixed complex containing 60−70% NAD^+ and 30−40% NADH. The crystals belong to the space group $P2_1$ with cell dimensions $a = 55.0$ Å, $b = 73.2$ Å, $c = 92.5$ Å, and $\beta = 102.5°$. A 98% complete data set to 1.54-Å resolution was collected at 100 K using synchrotron radiation. The structure was solved by the molecular replacement method utilizing EE-ADH as the search model. The major structural difference between the isozymes is a widening of the substrate channel. The largest shifts in C_α carbon positions (about 5 Å) are observed in the loop region, in which a deletion of Asp115 is found in the SS isozyme. SS-ADH easily accommodates cholic acid, whereas steroid substrates of similar bulkiness would not fit into the EE-ADH substrate site. In the ternary complex with NAD^+/NADH, we find that the carboxyl group of cholic acid ligates to the active site zinc ion, which probably contributes to the strong binding in the ternary NAD^+ complex.

In horse liver, ethanol (EE-ADH)[1] and steroid (SS-ADH) metabolizing isozymes of alcohol dehydrogenase, ADH (EC 1.1.1.1), are found together with the hybrid dimer, ES-ADH (*1*, *2*). Differences in coenzyme binding properties between the isozymes were first reported by Theorell et al. (*3*), and preliminary sequence information indicated that six amino acid substitutions, resulting in charge differences, distinguish the E- from the S-chain (*4*). The correlation between the changed sequence to the tertiary structure of EE-ADH (*5*) suggested that exchange of $Phe_{EE}110$ (lining the substrate pocket) for $Leu_{SS}110$ was the explanation for the differences in substrate specificity between the isozymes (*6*). From the cDNA sequence (*7*) and the complete amino acid sequence (*8*), a total of 10 amino acid changes between the E- and S-chains were finally identified, including the deletion of $Asp_{EE}115$ located in the substrate-binding region. Substrate specificity of ADH is governed by design of the substrate channel, which is created during dimer formation by residues originating from both subunits. Brändén (*9*) assigned Leu116 as the side chain hindering binding of steroid substrates to EE-ADH. Park and Plapp (*10*) proved by site-directed mutagenesis that deletion of $Asp_{EE}115$ rendered the mutated enzyme active toward steroid substrates.

Only the S-subunit can convert 3β-hydroxysteroids (Scheme 1), which are large and bulky substrates, whereas ethanol is a substrate for all three isozymes of ADH. A recent reexamination and detailed comparison of all rate constants, measured under standardized conditions, for NAD^+/NADH

[†] This work was supported by the University of the Saarland and the European Commission, Grant numbers BIO4-CT96-0189 and ERBFMGE-CT98-0134.

* To whom correspondence should be sent: Hans-Werner Adolph, Fachrichtung 8.8 Biochemie, Universität des Saarlandes, D-66041 Saarbrücken, FRG; phone: 49-681-3022492; fax: 49-681-3022097; e-mail: hwadolph@rz.uni-sb.de. Eila Cedergren-Zeppezauer, Department of Biochemistry, Center for Chemistry and Chemical Engeneering, Lund University, P.O. Box 124, S-22100 Lund, Sweden; phone: 46-462228178, fax: 46-462224534, e-mail: eila.cedergren@biokem.lu.se.

[‡] Universität des Saarlandes.

[§] EMBL.

[||] Lund University.

[#] Present address: Biochemistry, Biomedical Center, Uppsala University, S-75123 Uppsala, Sweden.

[1] NAD^+/NADH, oxidized/reduced nicotinamide adenine dinucleotide; EE-ADH, ethanol metabolizing alcohol dehydrogenase from horse liver (EC 1.1.1.1); SS-ADH, steroid metabolizing alcohol dehydrogenase from horse liver; YADH, yeast alcohol dehydrogenase; cholic acid, 3α,7α,12α-trihydroxy-5β-cholan-24-acid; A-3-ol, 5β-androstane-3β,-17β-ol; A-3-one, 5β-androstane-17β-ol-3β-one; PEG, poly(ethylene glycol); rmsd, root-mean-square deviation.

10.1021/bi001376s CCC: $19.00
Published on Web 09/29/2000

Scheme 1: Examples of Steroid Substrates and One Inhibitor of SS-ADH[a]

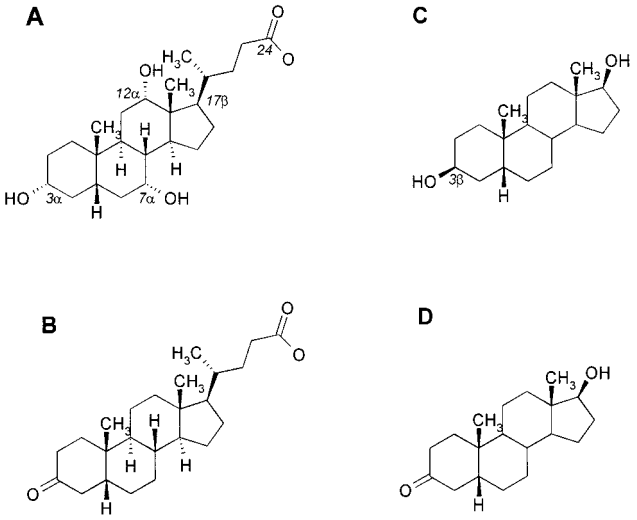

[a] (A) 3α,7α,12α-trihydroxy-5β-cholan-24-acid (cholic acid; inhibitor); (B) 5β-cholanoic acid-3-one; (C) 5β-androstane-3β-17β-ol (A-3-ol); (D) 5β-androstane-17β-ol-3-one (A-3-one).

binding to EE- and SS-ADH resulted in a two-step binding model in which adenine association/dissociation was separated from the nicotinamide docking/release process (*11*). Binding rates for the adenosine part of the coenzymes are significantly faster for the SS-ADH as compared to the EE-isozyme. Amino acid substitutions are found that lead to charge changes at the rims of the large coenzyme binding clefts. The overall charge difference between SS- (I_p above 10) and EE-ADH (I_p = 8.2) is +6 units. A "global" electrostatic field effect as a steering force has been suggested rather than assigning specific side chains in the protein being responsible for the pH dependencies of NAD^+/NADH binding.

This work presents the first X-ray structure of SS-ADH in complex with NAD^+/NADH and cholic acid (Scheme 1, structure A). Cholic acid is a potent inhibitor of SS-ADH in the presence of NAD^+ and differs only in the position of the 3-hydroxyl group from a 3β-hydroxy steroid substrate. Since cholanoic acid derivatives such as 5β-cholanoic acid-3-one (Scheme 1, structure B) are substrates for the SS-enzyme (*10*), we selected a similar compound for the X-ray determination of the substrate analogue complex. Furthermore, an extended analysis of substrate interactions has been made based on methods developed earlier for the EE-isozyme (*12*). This allows a direct comparison of individual rate constants of the underlying ordered bi-bi mechanism. The differences in substrate specificity and stereoselectivity between EE- and SS-ADH are described here on the basis of a comparison of 3D structures for both isozymes.

MATERIALS AND METHODS

Materials. Horse liver alcohol dehydrogenase isozymes were prepared as described by Hubatsch et al. (*13*). The characterization of isozymes, the purification of substrates, cofactors, buffers, and inhibitors have been described earlier (*11*, *12*, *14*). (4R)-(^{2}H)NADH, used to determine the primary kinetic isotope effect of ketone reduction, was prepared by a procedure similar to that described by Viola et al. (*15*).

Spectroscopy. Spectrophotometric measurements on single crystals were performed using an UMSP microspectrophotometer (Zeiss). Spectra were recorded using crystals mounted in a sealed X-ray capillary.

Kinetic Measurements. The kinetic experiments were carried out at 25 ± 0.5 °C in 0.1 M TAPS/KOH, pH 8.5, or 0.1 M TES/KOH, pH 7.0. For steady-state kinetics, the spectrophotometer Lambda 9 (Perkin-Elmer, Überlingen) was used. Fast kinetic measurements were carried out on a stopped-flow photometer system, model SHU SF-51 from HiTech Scientific. Experimental details have been described earlier (*12*). The single-turnover experiments with the SS-isozyme were followed fluorimetrically (excitation 340 nm, emission > 450 nm, detecting the formation or disappearance of NADH). To improve the signal-to-noise ratio, 5−8 reaction traces were averaged before fitting to single-exponential functions. The buffers used for kinetic measurements with the hydrophobic steroid substrates contained 2% acetonitrile for solubilization. Enzyme and coenzyme were premixed in one syringe, and substrate and inhibitor were added from a second syringe.

Theoretical Background for the Calculation of the Individual Rate Constants. For an ordered bi-bi mechanism (Scheme 2) the steady-state parameters k_{cat} and K_m for both

Scheme 2: Ordered Bi-Bi Mechanism for the ADH-Catalyzed Reaction[a]

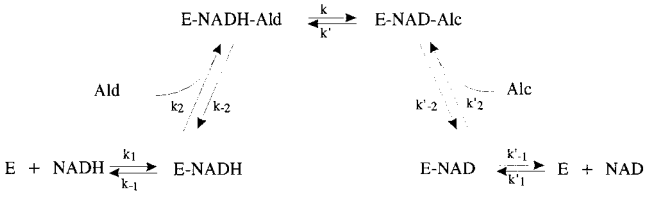

directions of a reaction are determined by the dissociation rate constants of the coenzymes [k_{-1}(NADH), k'_{-1}(NAD^+)], the association (k_2, k'_2), dissociation (k_{-2}, k'_{-2}), and hydride transfer (k, k') rate constants of aldehydes/ketones (Ald, Ket) and the corresponding alcohols (Alc), respectively, according to eqs 1−4 (*16*).

$$K'_m(\text{Alc}) = \frac{k_{-1}(k'_{-2}\,k + k'_{-2}k_{-2} + k'k_{-2})}{k'_2(k'k_{-2} + k'k_{-1} + kk_{-1} + k_{-1}k_{-2})} \quad (1)$$

$$k'_{cat}(\text{Alc}) = \frac{k'k_{-2}k_{-1}}{k'k_{-2} + k'k_{-1} + kk_{-1} + k_{-1}k_{-2}} \quad (2)$$

$$K_m(\text{Ald,Ket}) = \frac{k'_{-1}(k'_{-2}k + k'_{-2}k_{-2} + k'k_{-2})}{k_2(kk'_{-2} + kk'_{-1} + k'k'_{-1} + k'_{-1}k'_{-2})} \quad (3)$$

$$k_{cat}(\text{Ald,Ket}) = \frac{kk'_{-2}k'_{-1}}{kk'_{-2} + kk'_{-1} + k'k'_{-1} + k'_{-1}k'_{-2}} \quad (4)$$

Provided the hydride transfer rate constants are determined experimentally in combination with the steady-state parameters ($k^{(\prime)}_{cat}$, $K^{(\prime)}_m$) and the dissociation rate constants of the coenzymes ($k^{(\prime)}_{-1}$) the four rate constants for association ($k^{(\prime)}_2$) and dissociation ($k^{(\prime)}_{-2}$) of substrates, which are not

Scheme 3: Ordered Bi-Bi Mechanism for the Substrate System *R*-2-butanol (*R*-2-BuOH), *S*-2-butanol (*S*-2-BuOH)/2-butanone (2-BuO)[a]

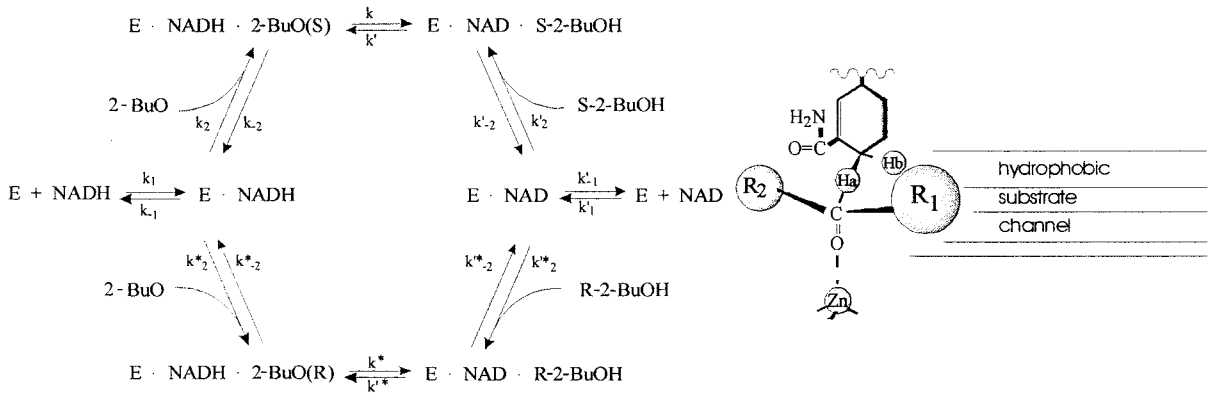

[a] The schematic representation in the inset illustrates the stereochemistry of hydride transfer between NADH and an aldehyde or ketone. In ADH-catalyzed reduction of aldehydes, R_1 represents the alkyl side chain, and R_2 represents a hydrogen. In case of for example, 2-butanone reduction binding with $R_1 = -C_2H_5$ and $R_2 = -CH_3$ (pro-S configuration) leads to formation of *S*-2-butanol.

accessible experimentally, can be calculated according to eqs 5−8 (*12*).

$$k_2 = \frac{k'_{-1}(k'_{-2}k + k_{-2}k'_{-2} + k'k_{-2})}{K_m(kk'_{-2} + kk'_{-1} + k'k'_{-1} + k'_{-1}k'_{-2})} \quad (5)$$

$$k_{-2} = -\frac{(k'_{cat}k'k_{-1} + k'_{cat}kk_{-1})}{(k'_{cat}k' + k'_{cat}k_{-1} - k'k_{-1})} \quad (6)$$

$$k'_2 = \frac{k_{-1}(k'_{-2}k + k_{-2}k'_{-2} + k'k_{-2})}{K'_m(k'k_{-2} + k'k_{-1} + kk_{-1} + k_{-1}k_{-2})} \quad (7)$$

$$k'_{-2} = -\frac{(k_{cat}kk'_{-1} + k_{cat}k'k'_{-1})}{(k_{cat}k + k_{cat}k'_{-1} - kk'_{-1})} \quad (8)$$

Since the two pathways for 2-butanone reduction (Scheme 3) cannot be studied separately, it is only possible to determine apparent k_{cat}, K_m, and k values, combining contributions of both pathways. Thus, the differential equation system is under-determined for a direct calculation of the missing rate constants [$k^{(\prime)}_{(-)2}{}^{(*)}$]. Additional experimental data or assumptions are necessary to solve this problem.

As shown earlier for the EE-isozyme (*12*), the free energy of activation for the hydride transfer step as well as the binding energy of the ketone substrates change systematically with systematic change in substituent size (R_1 and R_2 in Scheme 3). EE-ADH converts 2-butanone into 81% *S*- and 19% *R*-2-butanol under single turnover conditions. This allows the assumption that steady-state and single-turnover kinetics of 2-butanone reduction approximately reflect the production of *S*-2-butanol. From the data obtained for acetone, 3-pentanone, and the (pro-S) reduction of 2-butanone, the remaining unknown parameters for the (pro-R) reduction of 2-butanone can be estimated from free energy calculations (*12*) finally resulting in a complete set of rate constants for Scheme 3.

In case of the SS isozyme, an independent observation of only one pathway for 2-butanone reduction proved to be impossible since the product composition after single-turnover resulted in 56% *S*- and 44% *R*-2-butanol. From this finding, it was assumed that $k_{cat}{}^{(*)}$ and the hydride transfer rate constants [$k^{(*)}$] for pro-S and pro-R reduction both equal the experientally determined values (compare Tables 3 and 4). Accepting this approximation, all the dissociation rate constants of substrates [$k^{(\prime)}_{-2}{}^{(*)}$ in Scheme 3] can be calculated using the experimental data according to eqs 6 and 8. Additionally, the association rate constants for the enantiomeric alcohols can be estimated using eq 7. For the calculation of the association rate constants of 2-butanone to form the two alternative productive ternary complexes (k_2 and k_2* in Scheme 3), the individual K_m values for the two alternative pathways are needed. The enantiomeric ratio after 2-butanone reduction reflects the ratio of the k_{cat}/K_m values for both pathways (*12*) and gives [k_{cat}/K_m(pro-S)]/[k_{cat}/K_m-(pro-R)] = 1.228. Additionally, the experimental K_m equals [K_m(pro-S) + K_m(pro-R)]/2. Since the k_{cat} values are assumed to be identical, the individual K_m values can be calculated [K_m(pro-S) = 0.898K_m(experimental); K_m(pro-R) = 1.102K_m-(experimental)] and eq 5 can be solved.

Determination of Stereoselectivity of 2-Butanone Reduction under Kinetic and Thermodynamic Control. The reactions under single-turnover conditions (kinetic control) were carried out in 0.1 M TAPS, pH 8.5, 25 °C, and monitored at 340 nm with 2 mM pyrazole added. This excludes the back reaction since a strong complex with pyrazole and the NAD^+ product is formed at the active site (*17*). The experiments were carried out with 3.55 mM 2-butanone, 0.24 mM NADH, and 0.175 mM enzyme (EE- or SS-isozyme). The reactions were completed within 15 min (EE-ADH) and 40 min (SS-ADH).

Preparative 2-butanone reductions under equilibrium conditions (thermodynamic control) were performed with 3.55 mM 2-butanone, 0.24 mM NADH, and 0.025 mM enzyme (EE- or SS-ADH) for 6.5 h (EE-ADH) and 68 h (SS-ADH) without addition of pyrazole. For all experiments, controls without ketone were run in parallel. The reactions were stopped by freezing the resulting solutions in liquid nitrogen.

To avoid interference with the quantitative analysis of the enantiomeric composition of 2-butanol, coenzymes, enzymes, and pyrazole were removed by the following protocol: The solutions (1 mL) resulting from the reductions were distilled at 40 °C under reduced pressure. The procedure was repeated with the distillate, without heating, after acidification with 6 μL of H_2SO_4/mL of solution to ionize pyrazol and avoid its sublimation. The resulting distillate contained a mixture

of unreacted ketone and both enantiomers of 2-butanol. The amount of the *S*-enantiomer produced was selectively determined by quantitative oxidation with yeast alcohol dehydrogenase (YADH) which does not accept the *R*-enantiomer as a substrate. The combined amount of both enantiomers was determined with EE-ADH which accepts both *R*- and *S*-alcohols as substrates. The oxidation reactions were performed in 0.1 M glycine/KOH buffer, pH 10, containing 5 mM NAD^+ and enzyme (100 μM YADH or 40 μM EE-ADH) monitoring NADH production at 340 nm. The reactions were initiated by addition of 120 μL of the corresponding distillates to a final volume of 1 mL. Under these conditions, complete oxidation of the alcohols was achieved within 35 min. Since blank reactions could not be excluded completely, the corresponding reactions were additionally run without addition of the enantiomer mixture. The enantiomeric composition was finally calculated using eq 9:

$$[\Delta A_{(\text{YADH, analytical})} - \Delta A_{(\text{YADH, blank})}]/[\Delta A_{(\text{EE-ADH, analytical})} - \Delta A_{(\text{EE-ADH, blank})}] = [S\text{-2-butanol}]/([S\text{-2-butanol}] + [R\text{-2-butanol}]) \quad (9)$$

Simulation of Ketone Reduction. Mathematical simulations of the time course of 2-butanone reductions were performed with the stochastic simulation program "Chemical Reaction Simulator (CKS)" (*18*), applying the catalytic mechanism shown in Scheme 3 and the rate constants listed in Tables 3 and 4.

Crystallization and X-ray Data Collection. SS-ADH and its complexes easily crystallize under various conditions over a wide pH range (6−9.5). However, the crystals invariably grow as thin rods or sheets of a maximum thickness of about 0.01 mm. By balancing the proportions between low (PEG400) and high (PEG8000) molecular weight PEGs as precipitating agent, keeping neutral pH (I_p of SS-ADH is above 10) and low protein concentration, the thickness could be improved. The crystal used for the X-ray experiment was about 0.05-mm thick and harvested from a sitting drop in a micro bridge (Crystal Microsystems, K. Harlos, Oxford, UK). When mixed, the droplet contained 15 μL of protein solution (4 mg/mL) plus 15 μL of reservoir solution containing 4 mM NAD^+ and 5 mM cholic acid dissolved in 20% PEG400/10% PEG8000 in 0.1 M TES/KOH, pH 7.0. The drop equilibrated against 800 μL of reservoir solution, and crystals grew during several weeks. A fragment (0.2 × 0.1 × 0.05 mm) cut out from a 1-mm rod-shaped crystal was transferred to a cryo-protecting solution (same buffer containing 44% PEG400/5% PEG8000), mounted on a loop (*19*) and flash-frozen in a nitrogen stream. X-ray intensities were collected at 100 K on the beam line BW7B ($\lambda = 0.8373$ Å) at EMBL, Outstation Hamburg, equipped with a 300-mm Mar scanner (MAR X-RAY Research GmbH, Hamburg). Table 1 summarizes data statistics.

Data Processing, Structure Solution, and Refinement. Data were processed using the HKL-suite (*20*). Radiation damage due to the high brilliance of the beam, could not be prevented, although the data were collected under cryo-conditions. This is probably reflected in the high R_{merge} value (Table 1). Two percent of the processed independent reflections were excluded for R_{free} (*21*) calculations during refinement. The structure was solved by the molecular replacement method using the program AMORE (*22*), and a crystal structure of EE-ADH, in complex with NADH, refined at high resolution was used as the search model (Meijers et al., unpublished results).

Table 1: Statistics of Data Collected on the SS-ADH−NAD(H)−cholic Acid Complex[a]

space group	$P2_1$
unit cell (Å)	55.03, 73.17, 92.49, $\beta = 102.5°$
overall resolution range (Å)	20−1.54
no. of independent reflections	103 854
redundancy	4.16
completeness (%)	98.3 (97.2 for the highest shell)
R_{merge} (I%)	10.6 (25 for the highest shell)
$\langle I/\sigma I\rangle$	10.9 (4.5 for the highest shell)

[a] I is defined as $\Sigma_h\Sigma_i|I_{hi} - (I_h)|/\Sigma_h\Sigma_i|(I_h)|$ were I_{hi} is the intensity of the ith measurement of a reflection and (I_h) is the mean intensity observed for that reflection.

Table 2: Quality of the Model Obtained for the SS-ADH Complex

Refinement	
final *R*-factor	14.8% (14.5% before including R_{free} reflections)
R_{free} (2% of data)	18.3%
coordinate error (Å)	0.032 from ML[a] estimation
	0.068 from Cruickshank DPI[b]
Rms deviations	
1−2 distances	0.020 (target value 0.020)
1−3 distances	0.037 (target value 0.040)
Mean atomic displacement parameters [Å^2]	
B-factors from Wilson plot (Å^2)	14.1
for all atoms	16.7
protein atoms only	14.5
Zn (4 atoms)	12.2
cholic acid	16.0
NAD/NADH	11.2
waters (1150 atoms)	31.2

[a] ML = maximum likelihood. [b] DPI = dispersion precision indicator.

Automatic refinement was alternated with manual model building using the graphics program O (*23*). Maximum likelihood refinement of the model against the X-ray data was carried out with REFMAC (*24*). Restraints for the model were setup with PROTIN (*25*), and the program ARP (*26*) was used for automatic water building. A final refinement cycle was performed with the R_{free} reflections included, and the resulting model was validated with WHATIF (*27*, *28*). The average displacement factor for various subsets of atoms are listed in Table 2. The final model of the SS-ADH complex (R-value 14.8%) includes 5342 protein atoms (total 750 amino acids, 4 Zn ions, 2 coenzyme and 2 cholic acid molecules, the ligands estimated to have full occupancy). Coordinates have been deposited at the Protein Data Bank (PDB ID: 1EE2; RCSB ID: RCSB010481).

RESULTS

Substrate Specificity and Stereoselectivity of SS-ADH. The substrate specificity of SS-ADH was determined using secondary alcohols and their corresponding ketones. By systematically increasing the substituent size of substrates (R_1 and R_2 in Scheme 3) the interactions with the active site cavity of the enzyme could be probed.

Steady-state and rapid kinetic data for ethanol, various secondary alcohols and ketones, as well as 5β-androstane-3β,17β-ol (A-3-ol) and 5β-androstane-17β-ol-3β-one (A-3-

Table 3: Experimentally Determined Kinetic Constants for EE- and SS-ADH at pH 7.0 and 8.5

Kinetic Constants for EE- and SS-ADH

		k_{cat} [s^{-1}]		K_m [mM]		k_{cat}/K_m [$M^{-1} s^{-1}$]		k_H[d] [s^{-1}]		k_H/k_D[e]	
substrate	isozyme	pH 7.0	pH 8.5	pH 7.0	pH 8.5	pH 7.0	pH 8.5	pH 7.0	pH 8.5	pH 7.0	pH 8.5
ethanol	EE[a]	2.9	3.99	3.38	0.44	857	9068		150		
	SS[b]	1.05	1.24	36.5	1.80	29	694		110		
2-propanol	EE[a]	0.091	0.27	9.4	7.5	9.68	39	0.13	0.33		
	SS[b]		0.28		65		4.3				
acetone	EE[a]	0.056	0.067	53.3	66.0	1.05	1.02	0.057	0.070		
	SS[b]		0.11		1260		0.087				
S-2-butanol	EE[a]	0.42	1.0	0.51	1.35	823	740	1.90	2.50		
	SS[b]		0.62		10.7		57.9		5.65		
R-2-butanol	EE[a]	0.56	2.0	6.9	7.5	81.2	267	8.5	15.2		
	SS[b]		0.77		9.9		77.8		62.6		
2-butanone	EE[a]	0.10	0.12	11.4	15.0	8.77	8.00	0.131	0.122		3.30
	SS[b]		0.19		365		0.52		0.22		3.27
3-pentanol	EE[a]	0.83	2.26	2.1	1.6	394	1410	6.6	12.5		
	SS[b]		0.78		2.6		297		29.1		
3-pentanone	EE[a]	0.29	0.36	52.8	75	5.49	4.8	0.39	0.37		3.30
	SS[b]		0.24		149		1.6		0.24		3.38
A-3-ol	SS[b]	0.75	1.21	0.00142	0.00168	5.3×10^5	7.2×10^5	120	125		
A-3-one	SS[b]	3.54	0.62	0.0434	0.0649	8.16×10^4	9553	5.16	0.57	1.19	0.90

Coenzyme Dissociation Rate Constants ($k^{(\prime)}_{-1}$)[c]

coenzyme	isozyme	pH 7.0	pH 8.5
NADH	EE-ADH	2.15 s^{-1}	4.8 s^{-1}
	SS-ADH	1.05 s^{-1}	1.24 s^{-1}
NAD^+	EE-ADH	317 s^{-1}	32.4 s^{-1}
	SS-ADH	289 s^{-1}	30.0 s^{-1}

[a] The experimental data for EE-ADH at pH 8.5 are from ref *12*; the data for EE-ADH at pH 7.0 from ref *14*. [b] New data. [c] Data from ref *11*. [d] k_H is the hydride transfer rate constant obtained from single-turnover experiments. [e] k_H/k_D is the primary kinetic isotope effect obtained by single-turnover stopped-flow kinetics with NADH (k_H) and (4R)-(^{2}H)NADH (k_D) as the coenzymes.

Table 4: Calculated Rate Constants for Binding and Dissociation of Substrates, Substrate Dissociation Constants, and Hydride Transfer Rate Constants for EE- and SS-ADH at pH 7.0 and 8.5[a]

		k [s^{-1}]		k_2 [$M^{-1} s^{-1}$]		k_{-2} [s^{-1}]		K_d [mM]	
substrate	isozyme	pH 7.0	pH 8.5	pH 7.0	pH 8.5	pH 7.0	pH 8.5	pH 7.0	pH 8.5
(pro-S)- 2-butanone	EE	0.131	0.122	68.0	185	0.685	2.67	10.1	14.4
	SS		0.22		5.71		1.65		289
S-2-butanol	EE	1.9	2.5	4290	63600	6.78	203	1.58	3.19
	SS		5.65		511		39.0		76.2
(pro-R)- 2-butanone	EE	0.170	0.217	3.53	14.0	0.742	4.49	210	321
	SS		0.22		5.56		2.11		379
R-2-butanol	EE	8.5	15.2	852	23700	28.2	1280	33.1	53.8
	SS		62.6		651		417		641
A-3-on	SS	5.16	0.63	138000	nd	2.51	86.2	0.0182	nd
A-3-ol	SS	120	120	4360000	nd	285	nd	0.0653	nd

[a] The constants refer to Schemes 2 and 3.

one) are presented in Table 3 and compared to the EE isozyme for which the experimental data have been published earlier (*12*, *14*). The substrate specific rate constants from Schemes 2 and 3 for an ordered bi-bi mechanism are compared for SS- and EE-ADH in Table 4. The calculations of the corresponding individual rate constants for EE-ADH (Table 4) are based on dissociation rate constants for NAD^+ and NADH redetermined by Adolph et al. (*11*).

The stereochemical course of 2-butanone reduction under single-turnover conditions resulted in 81.3 (±0.5)% *S*-2-butanol and 18.7 (±0.5)% *R*-2-butanol for EE-ADH and 56.3 (±0.5)% *S*-2-butanol and 43.7 (±0.5)% *R*-2-butanol for SS-ADH. Obviously, the SS-isozyme shows a lower enantioselectivity for this reaction under kinetic control with the back reaction excluded since pyrazol is present. Under reaction conditions without an inhibitor added and long reaction times (equilibrium conditions), the product composition obtained is almost identical for both isozymes: 61.7 (±0.5)% *S*-2-butanol and 38.3 (±0.5)% *R*-2-butanol for EE-ADH and 63.2 (±0.5)% *S*-2-butanol and 36.8 (±0.5)% *R*-2-butanol for the SS-isozyme.

For the system *R*-2-butanol, *S*-2-butanol/2-butanone (Table 4) time courses of 2-butanone reduction were simulated using the program CKS. The simulations of the catalyzed reaction for a period of 6.5 h using the rate constants from Table 4 perfectly match the experimentally determined product compositions (Figure 1). The prediction of the equilibrium situation is highly consistent with experimental data and is an independent test of the reliability of the kinetic constants calculated from eqs 5−8.

The determinations of steady-state parameters for the oxidation of the steroid alcohol (A-3-ol) are approximate since substrate inhibition of SS-ADH is observed at high concentrations (data not shown). This inhibition is most likely

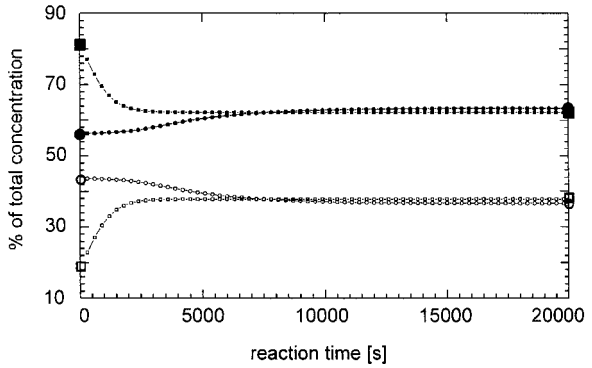

FIGURE 1: Stochastic simulation of 2-butanone conversion to *S*- and *R*-2-butanol catalyzed by EE- and SS-ADH. For the simulation, the reaction mechanism in Scheme 3 and the corresponding values for the rate constants from Tables 3 and 4 were used. Experimental data are symbolized by squares (EE-ADH) and circles (SS-ADH). Filled symbols represent *S*-2-butanol, open symbols *R*-2-butanol. At reaction time 0, the results represent the experimentally determined product composition after single-turnover reduction of 2-butanone. Data after 20000 s represent experimental data obtained under equilibrium conditions. The simulated time course of the percentual production of enantiomers is represented by small symbols.

due to formation of an abortive enzyme−NADH−alcohol complex which has also been described for the substrate ethanol with the EE-isozyme (*29*).

For the first time, rate constants for the catalytic step (k_H) of steroid substrate interconversion are presented (Table 3) together with primary kinetic isotope effects for the reduction of A-3-one by SS-ADH. Whereas the hydride transfer rate constant for the steroid alcohol (A-3-ol) is fast (120 s^{-1}) and comparable to the rate constant for ethanol conversion (110 s^{-1}), the catalytic step for ketone reduction (k), seems to be very slow (between 0.5 and 5 s^{-1} over the pH range). The increase of k for A-3-one by 1 order of magnitude between pH 8.5 and 7.0 indicates that the experiments do not result in "true" hydride transfer rate constants, which is also reflected in the virtual absence of a primary kinetic isotope effect for this reaction step (discussed below).

Generally the "small" substrates, namely, ethanol, secondary alcohols, and ketones, show lower substrate specificity (k_{cat}/K_m) for the SS- as compared to the EE-isozyme. This results from generally lower k_{cat} and increased K_m values. For the catalytic step of the reaction, the difference in rate constants for the two isozymes is small whereas the oxidation of the secondary alcohols shows 2−4-fold increased hydride transfer rate constants for the SS-isozyme. The primary kinetic isotope effect for ketone reduction is virtually identical for both isozymes.

Microspectrophotometric Analysis of Single Crystals. The crystals of the SS-ADH/cholic acid/NAD complex were grown in the presence of NAD^+. The mother liquor was checked for the content of NADH by photometric analysis, and no absorption at 340 nm, typical for the reduced nicotinamide ring in solution, could be detected (Figure 2). To ensure whether the crystallographically studied complex in fact represented a pure NAD^+ species, single-crystal spectra were recorded between 450 and 240 nm on remaining fragments of the 1-mm crystalline rod used for data collection. An absorption maximum was observed (Figure 2) characteristic of NADH bound to the protein (*30*). From the relative absorbance, it can be estimated that 30−40% of the binding sites are occupied by NADH thus confirming

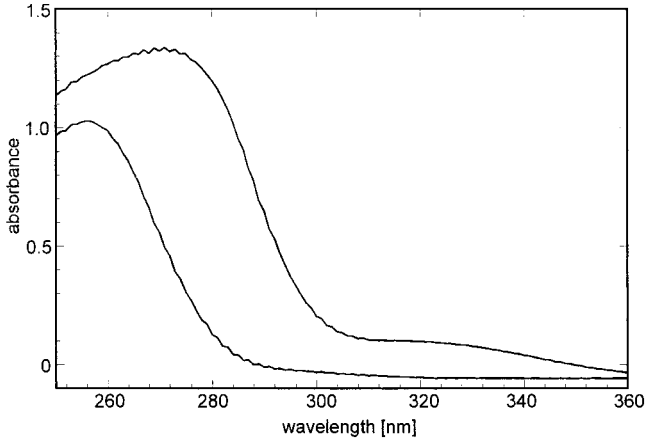

FIGURE 2: UV spectra of the crystal used for data collection (upper curve) and the surrounding mother liquor (lower curve).

that the structure presented in this work is a mixed NAD^+/NADH complex.

Crystals grow over several weeks, and, due to the presence of unidentified alcohol substrates for ADH in all PEGs tested (data not shown), formation of NADH can already occur before crystallization of the protein complex starts. Since NADH has a considerably higher affinity to the enzyme as compared to NAD^+ (*11*), even traces of NADH produced can cause considerable occupation of the enzyme. Our experience of getting a mixed NAD^+/NADH complex, when starting from a NAD^+-containing solution, might be extended to crystalline complexes of ADH and other dehydrogenases described in the literature.

Quality of the Electron Density Map. The electron density map of the ternary complex of dimeric SS-ADH is excellent, and the surface loop 113−118 is shown as an example of its quality (Figure 3). A few surface residues are not visible in density after the CG atom (mostly lysines) and these atoms were given zero occupancy in the PDB file. Several surface residues are observed, where double conformations are evident from the 1.54-Å resolution map, particularly Asp and Glu side chains.

Overall Structure. EE-ADH−coenzyme complexes in the closed enzyme conformation (*31*, *32*) are characterized by an 11° rigid body rotation of the catalytic domain about a hinge axis (*33*). This structural change, going from an open to a closed protein conformation, involves approximately 200 residues per monomer. The 10 amino acid substitutions in SS-ADH do not alter this feature, and the rotation angle about the hinge axis is 10°. The SS-ADH−NAD(H)−cholic acid complex described here has a similar overall structure as EE-ADH complexes in a closed enzyme form (Figure 4). However, local changes in the substrate channel are observed, which are described in detail below.

Coenzyme Binding. The electron density observed in the coenzyme binding site is clearly defined. The binding mode of NAD(H) in inhibited ternary complexes in the closed protein conformation is similar in the SS- and EE-isozymes although it is a mixture of oxidized and reduced cofactor (Figure 2).

Coenzyme interactions to the protein in various alcohol dehydrogenase complexes have been extensively described (*31*, *32*, *34*−*39*). The 10 amino acid changes in SS-ADH do not alter bonding interactions between the enzyme and

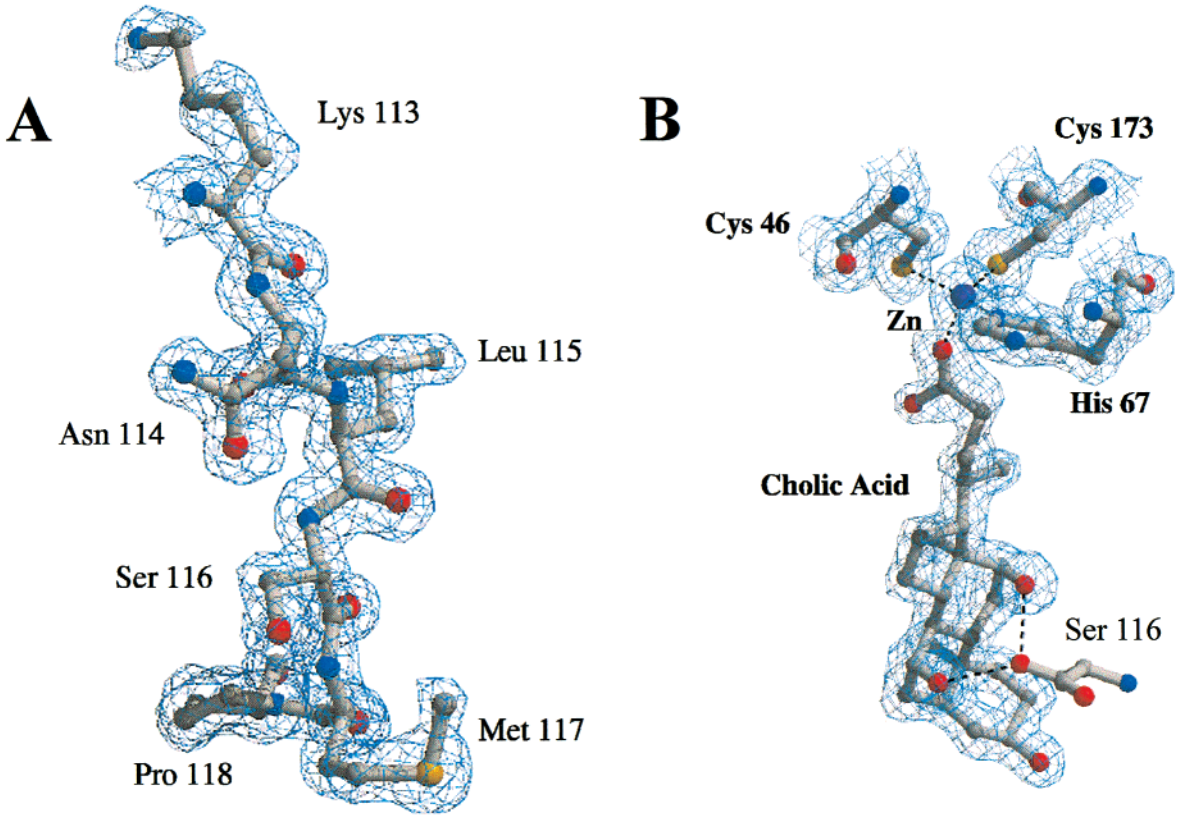

FIGURE 3: Quality of the electron density map. A $3F_0-2F_c$ electron density map is shown at 1.50 σ level with the models of (A) residues 113−118 and (B) cholic acid and the catalytic zinc ion with its protein ligands. Picture generated with BOBSCRIPT (*45*).

the cofactor when compared to the closed protein structure of EE-ADH. However, binding rates of coenzymes differ by an order of magnitude between the EE- and SS-isozymes (*11*) apparently due to the charge differences between isozymes.

Briefly, coenzyme binding to SS-ADH is mediated by charge interactions around the pyrophosphate bridge (Arg47 and Arg368), hydrogen bonds to main chain and side chain atoms around both ribose moieties and hydrophobic stacking involving the adenine ring. The Zn-coordination sphere (with the metal ligands Cys46, His67, and Cys173) is at van der Waals distance to the nicotinamide, facing the A-side of the ring, whereas the opposite side is totally hydrophobic. Ser48 assigned a crucial role in proton-transfer reactions is located next to the metal center and makes a short hydrogen bond to the O2′ of the nicotinamide ribose (2.6 Å). His51, proposed to be the second half of the proton relay system, has an unfavorable orientation to make a hydrogen bond to this ribose oxygen.

The coenzyme is surrounded by a large number of water molecules although the protein structure is in a closed conformation with the cofactor trapped in a narrow binding cleft. Water molecules firmly associated to the protein, having B-factors similar to protein atoms, mediate contacts to NAD(H) by the pyrophosphate bridge. $Lys_{EE}228$ has been shown by chemical modification to influence coenzyme dissociation in EE-ADH (ref *40* and references therein). This lysine side chain is mostly described as interacting with the adenosine ribose, but in the inhibited SS-ADH complex we observe that $Lys_{SS}227$ is only partially occupied in a position to bind to the O3′ atom of ribose. A water molecule substitutes NZ when the amino group is oriented in a different direction. NZ-227_{SS} shares its interactions between the ribose and the carbonyl oxygen of residue 366_{SS} of the catalytic domain across a cleft separating domains. The neighboring peptide flips upon domain rotation (*32*) induced by coenzyme complex formation. Thus, the role of the lysine side chain might be linked to the trigger mechanism of the conformation change in ADH.

Location of Amino Acid Substitutions. Table 5 lists the mutations converting the EE subunit to the SS form. Remarks are made on their effect on the charge of the protein and describe the location of the side chains with respect to substrate and cofactor positions. Figure 4 depicts the locations of the substitutions. Inspection of the SS-ADH structure indicates that two substitutions have no obvious influence on coenzyme binding or substrate interactions: Thr_{EE}-$278Ala_{SS}277$ and $Ile_{EE}172Val_{SS}171$. The remaining amino acid mutations influence various features: (i) the size of the substrate channel, (ii) the hydrophobicity of the substrate binding area, (iii) the charge distribution of the protein, and (iv) cause a large, local structural changes in a peptide loop, here denoted "the steroid binding loop" (residues 113−120).

The Major Structural Difference between EE- and SS-ADH. The substrate binding site in ADH is an elongated channel lined by residues originating from both subunits. This channel can be divided into three regions: the metal center (at which the substrate ligates to the Zn^{2+} ion), a central hydrophobic cavity (about 12-Å long), and, in a distance of 20 Å to the metal ion, a water-rich rim having hydrophilic, positively charged side chains.

A certain flexibility of hydrophobic side chains allows for a limited variation in the shape within the central "compartment". This is observed in the SS-ADH−coenzyme−cholic

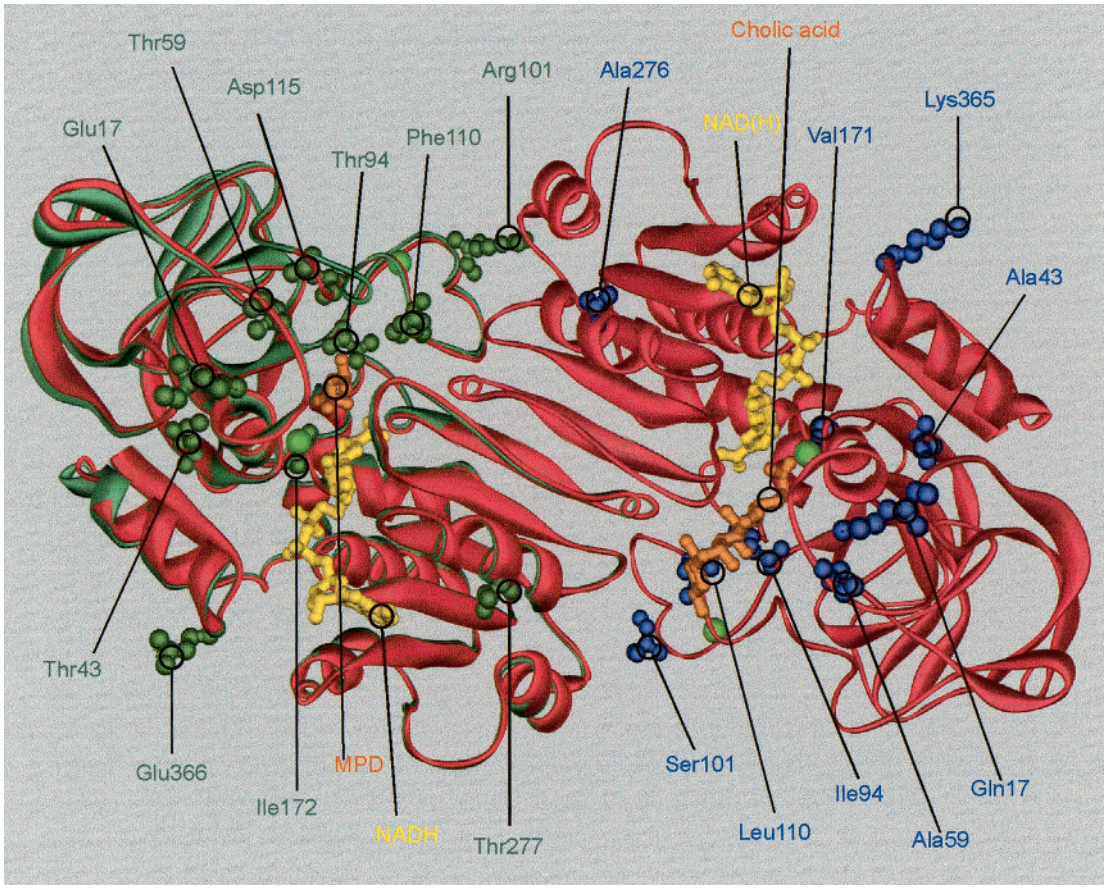

FIGURE 4: Comparison of the overall structures of EE- and SS-ADH. For the alignment, a structure of the EE-ADH−NADH−MPD complex at 1.0-Å resolution was used (Meijers et al., 2000). The whole SS-ADH dimer (red) and one monomer of EE-ADH (green) are shown. The structural comparison of the isozymes is based on an alignment of atom positions for the coenzyme binding domains of the A subunit (right) of both isozymes. The mutated side chains are shown as ball-and-stick models in blue (SS-ADH) and green (EE-ADH). The locations of NAD(H) (yellow) and cholic acid (orange) in the S subunit and NADH (yellow) and MPD (orange) in the E subunit are represented as ball-and-stick models. Picture generated with Weblab Viewer (MSI, Incorporated).

Table 5: Description of Location and Effect of Amino Acid Substitutions between EE- and SS-ADH.

residue	effect of substitution	location in relation to cofactor/substrate
17 Glu_{EE}-Gln_{SS}	negative charge lost	at the rim of the nicotinamide subsite of the coenzyme binding cleft
43 Thr_{EE}-Ala_{SS}	H-bond lost; smaller volume of group	buried behind the active site zinc ion; new water added to an interior cavity
59 Thr_{EE}-Ala_{SS}	H-bond lost; smaller volume	not in direct contact with substrate
94 Thr_{EE}-Ile_{SS}	H-bond lost; larger volume	increased hydrophobicity of substrate channel
101 Arg_{EE}-Ser_{SS}	positive charge lost	no direct interaction with substrates
110 Phe_{EE}-Leu_{SS}	smaller volume of group	increased volume of substrate channel
115 Asp_{EE}-$deletion_{SS}$	negative charge lost	centre of substrate binding site inducing large conformational change in a loop
172 Ile_{EE}-$Val_{SS}171$	smaller volume of group	remote from active site in hydrophobic interior
277 Thr_{EE}-$Ala_{SS}276$	H-bond lost; smaller volume	remote from active site
366 Glu_{EE}-$Lys_{SS}365$	negative charge changed to positive	at the rim of the adenine subsite of the coenzyme binding cleft

acid complex in which Ile94 occupies alternative positions. Side chain disorder in the hydrophobic region is also observed in the EE-isozyme (*41*). $Met_{EE}306$ is a good example. It protrudes into the substrate channel from the other subunit. At a particular orientation, this bulky side chain can restrict accessibilty into the metal site. Furthermore, the location of Phe110 and Leu116 in EE-ADH limit the compartment size to better fit smaller substrates rather than steroids (Figure 5, panel A).

The mutation having the largest impact on the change in size of the substrate channel in SS-ADH is the deletion of $Asp_{EE}115$ (Figure 5, panel B). The substitution Phe_{EE}-$110Leu_{SS}$ also contributes to the widening of the site, but truncation of the loop 113−120 involves a rearrangement of main chain atom positions up to 5 Å, generating a larger volume going from 250 $Å^3$ in EE-ADH to 500 $Å^3$ in the SS isozyme. The position of $Asp_{EE}115$ is inside the loop (Figure 5, panel A) to which the carboxyl group forms hydrogen bonds to main chain amide nitrogens. $Leu_{EE}116$, which occupies a volume in the vicinity of the active site metal, becomes buried inside the truncated loop (Figure 5, panel B). Because of the rearrangement of residues 113−120 now $Ser_{SS}116$ is able to interact with cholic acid or a steroid substrate (Figure 3). Interaction of $Ser_{EE}117$ with small substrates is unlikely due to the long distance to the inner compartment of the substrate channel.

Cholic Acid Binding. The inhibitor molecule was clearly defined by the difference density map calculated before the inhibitor model was introduced in the refinement. Figure 3 shows the density after the refinement had converged.

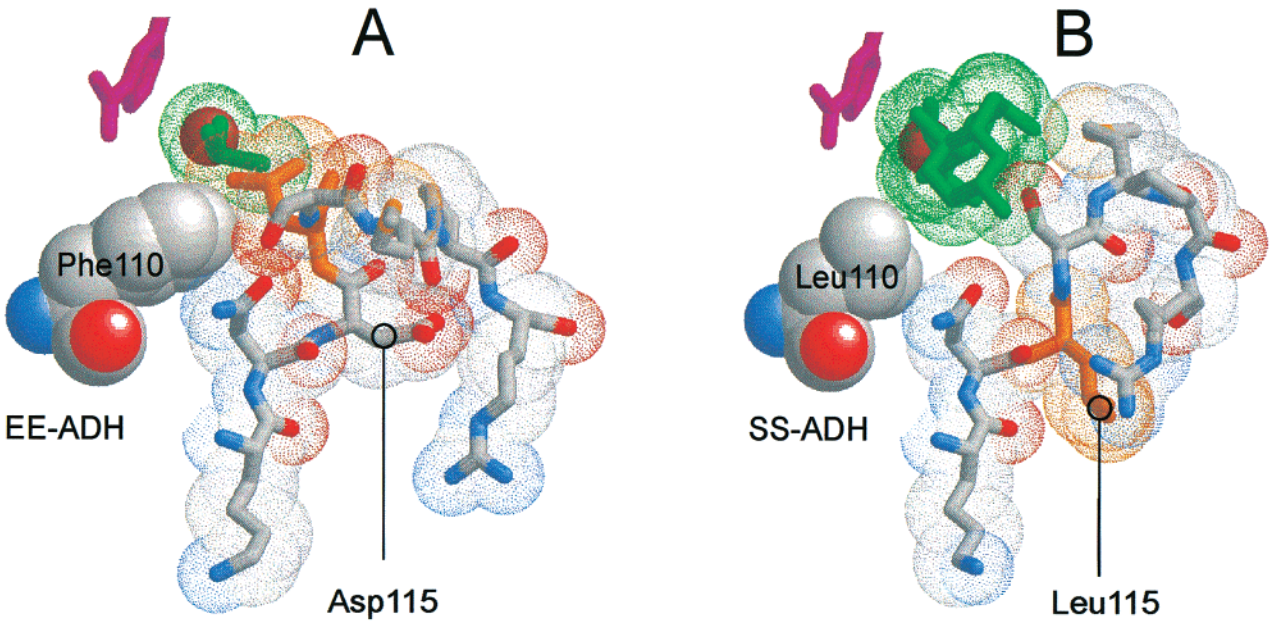

FIGURE 5: Comparison of the entrance to the inner compartment of the substrate channel in EE- and SS-ADH. Figure produced with Rasmol 5.0 (*46*). (A) Represents the structure of the EE-ADH−NADH−DMSO complex at 1.8-Å resolution (PDB accession number: 2ohx) (*32*). The dihydropyridine ring is in magenta and DMSO in green. $Leu_{EE}116$ (yellow) is closest neighbor to DMSO and $Phe_{EE}110$ (space-filling model) blocks the entrance into the interior of the substrate channel. (B) The same region of the SS-isozyme in an identical orientation. $Leu_{SS}115$ (yellow) now takes the position of the deleted $Asp_{EE}115$ after a conformational change in the loop. The Phe_{EE}-$110Leu_{SS}$ mutation further enlarges the active site allowing the bulky cholic acid (green) to dock.

Table 6: Zn Ligand Distances and Angles

	B-subunit	A-subunit
bond length [Å]		
Zn-Nϵ67	2.08	2.02
Zn-Sγ46	2.40	2.37
Zn-Sγ173	2.23	2.27
Zn-O26(cholic acid)	2.11	2.00
bond angle [°]		
Nϵ67-Zn-Sγ46	107	107
Nϵ67-Zn-O26 (cholic acid)	103	99
Nϵ67-Zn-Sγ173	115	117
Sγ46-Zn-Sγ173	121	120
Sγ46-Zn-O26(cholic acid)	101	102
Sγ173-Zn-O26(cholic acid)	106	108

The cholic acid molecule occupies the full length of the substrate channel. $Glu_{SS}283$ (from the second subunit) and $Asn_{SS}114$ (from the steroid binding loop) sit as "gate keepers" at the entrance into the cylindrical, hydrophobic cavity. Lys_{SS}-113 and $Arg_{SS}119$ which are situated at the start and end of the steroid binding loop make the surface positively charged. In the steroid ring skeleton (Scheme 1) the 3α-hydroxyl group of ring I is directed to this hydrophilic environment and not toward the metal center. This was unexpected since 3*β*-derivatives are substrates. The 3α-hydroxyl group makes no direct interactions to the side chains in its neighborhood but only to water molecules. Instead, O26 of the carboxyl group at the opposite end of the four-membered ring system (Scheme 1) is the ligand to the zinc ion (bond length 2.1 Å). O25 and O26 are at hydrogen bonding distance to Ser48. Table 6 summarizes bond lengths and bond angles for the active site metal ion in both subunits. The coordination geometry of zinc in the A and B subunit is nearly identical and not so heavily distorted from a tetrahedral geometry as found for other complexes of LADH (*41*).

The hydrophobic ring system is pushed far out along the apolar region of the channel due to the length of the C17-substituent carrying the carboxylate. Methyl substituents on the cholic acid molecule are directed to one surface of the hydrophobic channel ($Met_{SS}305$ and $Leu_{SS}308$, second subunit), the two hydroxyl substituents at positions 7α and 12α in ring II and III (Scheme 1) interact with $Ser_{SS}116$ on the steroid binding loop. Nine hydrophobic side chains are at van der Waals distance to the ring system all together. Thus, the cholic acid inhibitor is firmly anchored through the metal−ligand bond, by hydrogen bonds to hydroxyl substituents and by numerous hydrophobic interactions.

DISCUSSION

The present X-ray structure of the steroid-active isozyme of horse liver alcohol dehydrogenase (SS-ADH) at 1.54-Å resolution allows a detailed analysis of the structural and functional consequences of the 10 amino acid mutations since the EE isozyme is structurally well-characterized. A direct comparison of the isozymes with regard to the effects of local structural changes in the protein on the kinetic characteristics further allows an explanation of observed differences in substrate specificity and stereoselectivity. Whereas the gross structural organization of both isozymes is almost identical, the substitutions in the E-chain result in three types of effects: (i) an increased size of the substrate channel combined with (ii) an increased hydrophobicity of the substrate binding area and (iii) a drastic increase of the net charge (+ 6 units) combined with an altered charge distribution on the protein surface.

The amino acid substitutions are scattered over a wide region on the catalytic domain (Figure 4) with the exception of $Thr_{EE}277Ala_{SS}276$ which is located at a helix forming part of the adenine binding pocket. Most mutations are located along that surface of the catalytic domain which forms the ligand binding crevices. This surface is at the "ligand entrance face" (Figure 4) in contrast to the "back" of the

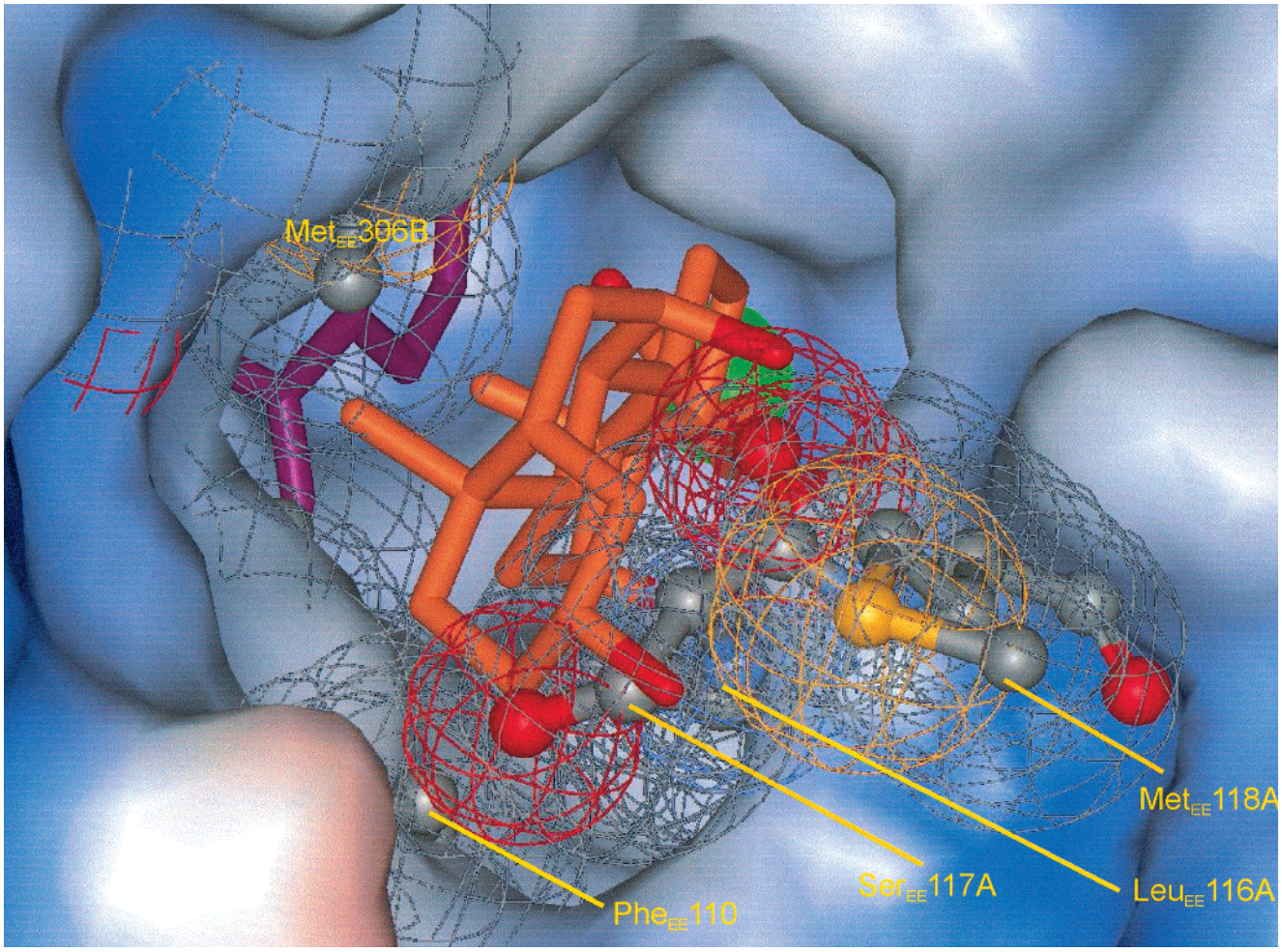

FIGURE 6: Comparison of the substrate channel architecture of SS- and EE-ADH. The structural alignment is described in the legend of Figure 4. The solvent-accessible surface of the substrate channel of SS-ADH is shown with the catalytic zinc ion (green) on the bottom after the channel. The nicotinamide of bound coenzyme (magenta) and the cholic acid molecule (orange) are represented as stick models. The ball-and-stick models severely colliding with cholic acid represent side chains of the superimposed EE model. The van der Waals contact radii of protruding groups are indicated as mesh surfaces, which partially penetrate the bound steroid molecule at various positions. Picture generated with Weblab Viewer (MSI, Incorporated).

molecule from which direction cofactor or substrate have no access.

The Ile$_{EE}$172Val$_{SS}$171 exchange cannot easily be assigned a functional role. As pointed out in Table 5, it is remote from the active site and the side chain is buried in a hydrophobic interior close to the C-terminus. A new cavity behind the metal coordination sphere is formed when Thr$_{EE}$-43 is substituted for an alanine. Inside this hydrophobic site a water molecule is replacing the hydroxyl position of Thr$_{EE}$-43. We speculate that these two substitutions might contribute to an observed destabilization of the SS-isozyme as compared to EE-ADH, which does not denature as readily.

What Makes SS-ADH a 3β-Hydroxy Steroid Dehydrogenase. The preliminary amino acid sequence of SS-ADH (*4*) suggested that the substitution Phe$_{EE}$110Leu$_{SS}$ made the enzyme accept the bulky steroid substrates although Brändén (*9*) pointed out that Leu$_{EE}$116 is hindering binding of steroids. After the complete amino acid sequence was available (*7*, *8*), it became obvious that the deletion of Asp$_{EE}$115 could be the most relevant structural change. This has been verified by site-directed mutagenesis proofing the Asp$_{EE}$115Δ$_{SS}$ mutant to be moderately active with 3β-hydroxy steroids (*10*). A direct structural comparison uncovers that all three effects mentioned above contribute to the adaption of the substrate channel in SS-ADH to accommodate steroid substrates (Figure 5). The surface representation in Figure 6 shows that five side chains of the EE-isozyme protrude the substrate channel surface of the SS isozyme when the structures are aligned. From this representation it becomes obvious that the substrate channel of EE-ADH is far too narrow to be able to bind a steroid substrate.

The Catalytic Step in Steroid Conversion. The catalytic efficiency of SS-ADH with A-3-ol as substrate is increased by 2−3 orders of magnitude as compared to ethanol as a substrate at pH 7.0 and 8.5, respectively. This is due to the stronger binding of the steroid substrate having a K_d of 65 μM at pH 7.0. The rate constant for the hydride transfer step during alcohol oxidation is almost identical for ethanol and A-3-ol (Table 3). The steroid ketone binds even stronger to the enzyme as compared to the alcohol whereas the catalytic efficiency of its conversion is lower. An attempt to measure the hydride transfer step from NADH to A-3-one in single-turnover experiments failed in the sense that the primary kinetic isotope effect for this reaction step proved to be close to 1 under the experimental conditions used (Table 3). Furthermore, a pronounced pH effect is observed for A-3-

one conversion between pH 8.5 and 7.0 indicated by an increase of the rate constant for the catalytic step by 1 order of magnitude. This is not observed in any other case for the EE-isozyme (Table 3). Since the disappearance of NADH is monitored fluorimetrically in the single turnover experiments the absence of a kinetic isotope effect means that the rate-limiting step for the reaction observed is different from hydride transfer. The pronounced increase of the rate constant observed at pH 7.0 and the primary kinetic isotope effect of 1.2 at pH 7.0 (which is still far from the value observed for the small aliphatic ketones) suggests that protonation of the zinc-bound alcoholate obtained after hydride transfer might be the rate-limiting step of the reaction. In this sense, the ordered bi-bi mechanism is a simplification combining hydride transfer and protonation/deprotonation in one reaction step.

Substrate Specificity with Small Secondary Alcohols and Ketones. The change of the substrate channel architecture in SS-ADH has a pronounced effect on the dynamics of substrate binding. The association rate constants (k'_2) of the 2-butanol enantiomers are reduced by 2 orders of magnitude and those for the ketone by 1 order of magnitude as compared to the EE isozyme (Table 4). This cannot be a consequence of a more difficult access to the substrate channel which has a 100% larger volume. That becomes obvious from a comparison of the corresponding rate constants for steroid substrates. The association rate constant for the steroid alcohol is 4.4×10^6 M^{-1} s^{-1} at pH 7.0 and thus 3 orders of magnitude higher as compared to the small secondary alcohols. This means that the major problem in docking of small substrates is not to find the active site but to form a productive ternary complex. The widening of the substrate channel might not allow for a proper steering in the docking process. Different conformations of the enzyme−substrate complex with nonproductive orientation might be possible due to a low energetic advantage of the productive conformation. The same holds for dissociation which is generally slower for SS-ADH. Since many possible interactions exist for the small hydrophobic products, the transfer to the bulk water is less likely from the SS-ADH active site which has a wider and more hydrophobic substrate channel.

Isozyme-Specific Differences in Stereoselectivity. The difference between yeast alcohol dehydrogenase (YADH), which exclusively accepts *S*-2-butanol, *S*-2-pentanol, and *S*-2-octanol and the horse liver enzyme, which also accepts the respective *R*-enantiomers, was first described by Dickinson and Dalziel (*42*). The first full account of the catalytic cycle (Scheme 3) for secondary alcohol/ketone substrate pairs indicated that the enantioselectivity of EE-ADH is based on differences in free energy of binding and activation of the alternative alcohol substrates or ternary complex configurations of the prochiral ketones (compare Scheme 3) (*12*). Those enantiomers that bind weaker show a lower activation barrier for hydride transfer. The present investigation confirms this effect for the SS isozyme (Table 4).

Similar observations have been reported for human ADH (*43*), and a pronounced role of residue 48 which is either Thr or Ser in the different human isozymes has been discussed. Site-directed mutagenesis of Thr48 in human $\beta\beta$-ADH to Ser rendered the enzyme active on steroids as well as cyclohexanol (*44*). For the horse liver enzyme, it can be concluded from the available structures that a Ser48Thr mutation would reduce the space in the active site such that binding of any secondary alcohol or ketone would be almost impossible in the closed conformation of the protein. A Thr48Ala mutant of the human enzyme was found to be completely inactive (*44*) underlining the crucial role of a side chain hydroxy group in position 48 for enzymatic activity.

Comparison of the "Inner Compartment" of the Substrate Channels. The aliphatic substituent in position 17 of the steroid polycycle is positioned in the binding region of the aliphatic substituent of a primary alcohol (*35*). C23 of cholic acid is located in the putative position of the methyl group of ethanol at van der Waals contact (4.1 Å) to CZ of Phe93. The noncoordinating oxygen (O25) of the carboxylate corresponds to the R_2-substituent depicted in Scheme 3. O25 is at van der Waals contact distance to CG of Val293 (3.62 Å) as well as the C4 and C5 atoms of the nicotinamide (3.51 and 3.84 Å, respectively). The orientation of the carboxylate group of cholic acid is a good model for a planar ketone substrate binding to the metal ion. The very close distance to Ser48, Val293, and the nicotinamide make it necessary for a R_2 substituent larger than one carbon atom to be oriented into the substrate channel. The distance measured between OG of Ser48 and CZ of Phe93 differ by 0.5 Å between the isozymes, giving more space for arranging the substituents on the carbonyl carbon. This might contribute to the result that the SS-isozyme does not discriminate between the pro-R and pro-S conformations of 2-butanone in terms of free energy of binding and activation. The K_d values calculated (Table 4) show equally weak binding for both conformers. The advantage of having a larger substituent in position R_1 of a ketone observed for EE-ADH is not seen with the SS-isozyme. With EE-ADH, the two possible productive ternary complexes with 2-butanone show a factor of 20 difference of K_d but only a factor of 2 difference of k in favor of the weaker binding conformation. SS-ADH almost does not discriminate between both pathways. This leads to the observed product composition after single turnover reduction with 81% *S*- and 19% *R*-alcohol in case of EE-ADH as compared to 56% *S*- and 44% *R*- with the SS isozyme. These results are obtained under exclusion of the back reaction.

Different from ketone substrates, examination of 2-butanol oxidation uncovers that both EE- and SS-ADH clearly distinguish between both enantiomers in terms of binding and activation. It can be assumed that R_1 of the tetrahedral alcohols will take the most advantageous position in the substrate channel and the R_2 substituent will approach Ser-48. Therefore, it seems reasonable that productive binding of *R*-2-butanol as compared to *S*-2-butanol causes sterical problems that are reflected in the higher K_d for both isozymes. Possibly the energetically unfavorable positioning of *R*-2-butanol results in an approach of the hydride ion to C4 of the nicotinamide reducing the free energy of activation for hydride transfer. With both isozymes, these effects are more pronounced for the alcohols. Under equilibrium conditions, where both directions of the reaction are relevant, the energetic differences for the secondary alcohol discrimination influence the final enantiomeric composition. As can be seen from the catalytic efficiencies (k_{cat}/K_m), EE-ADH favors oxidation of the *S*-enantiomer by a factor of 3 (Table 3). This means that the preferentially produced alcohol is oxidized faster than its counterpart resulting in a decreased

enantiomeric ratio under equilibrium conditions (1.5). In case of SS-ADH, a small preference for the reoxidation of the *R*-alcohol finally leads to an increased enantiomeric ratio under equilibrium as compared to single-turnover conditions (1.7 and 1.3, respectively).

Isozyme-Specific Differences in Substrate Specificity and Stereoselectivity are a Combined Effect of Electrostatic and Structural Changes. The influence of changes in the electrostatic properties of ADH isozymes on coenzyme binding have been discussed in detail (*11*). Inspection of coenzyme binding in SS-ADH (see Results) did not reveal any differences in NAD(H)−protein interactions between EE- and SS-ADH. Thus the conclusions drawn in ref *11* remain uncontradicted: The increased affinity of SS-ADH for NADH and NAD^+ reflects an increased electrostatic attraction of the negatively charged cofactors due to the increased net charge of the enzyme. Since the coenzyme binding dynamics is a major determinant for substrate kinetics of ADH, changes in the coenzyme binding kinetics have direct influence on the kinetics of substrate conversion.

A further analysis of the structural and functional significance of the various substitutions can now be made comparing kinetic parameters for native EE- and SS-enzymes with those of site-directed mutants investigated by Park and Plapp (*10*). Alone the $Asp_{EE}115$ deletion allows for a steroid substrate to bind. The K_m value for A-3-ol (Scheme 1) is 8-fold higher (*10*) as compared to the value for SS-ADH determined here (Table 3). Since the reorganization of the loop 113−120 is the major structural difference between native EE- and SS-ADH and contributes most to the enlargement of the substrate site, we expect this structural change to occur independent of the other substitutions. The remaining mutations close to the substrate binding site contribute to the fine-tuning of the optimization of channel size and hydrophobicity (residues 59, 94, and 110, see Table 5). In fact, a further decrease in K_m is observed by Park and Plapp (*10*) for the oxidation of A-3-ol when multiple mutations (94,101,110 plus the Asp115 deletion) are made. The finding of an increased catalytic activity of some of the mutants described by Park and Plapp (*10*) as compared to either EE- or SS-ADH toward primary alcohols and steroids can only be explained in terms of increased dissociation rate constants for the coenzymes. Now considering the two-step mechanism for coenzyme binding described in ref *11*, an accelerated release of the nicotinamide could be coupled to a protein conformational change. This step was found to be faster for SS-ADH possibly due to the reduced interactions between the two domains of the protein, although the overall dissociation rate constant of NADH and thus k_{cat} for ethanol are slower as compared to EE-ADH. Increased k_{cat} with ethanol is observed for a mutant (*10*) where only residues relevant for modification of the substrate channel were made. Thus mutations giving the SS-isozyme additional positive net charge seem to be necessary for compensation of the changes in the substrate channel with respect to coenzyme dissociation constants. As has been found for the so-called ESE mutant (*10*), the absence of the charge changes results in considerably weakened binding of the coenzymes.

ACKNOWLEDGMENT

We thank Z. Dauter for help in testing various crystal forms of SS-ADH at an early stage of this work.

REFERENCES

1. Pietruszko, R., Clark, A., Graves, J. M. H., and Ringold, H. J. (1966) *Biochem. Biophys. Res. Comm. 23*, 526−534.
2. Pietruszko, R., and Theorell, H. (1969) *Arch. Biochem. Biophys. 131*, 288−298.
3. Theorell, H., Åkeson, Å., Liszka-Kopec, B., and de Zalenski, C. (1970) *Arch. Biochem. Biophys. 139*, 241−247.
4. Jörnvall, H. (1970) *Eur. J. Biochem. 16*, 41−49.
5. Eklund, H., Nordström, B., Zeppezauer, E., Söderlund, G., Ohlsson, I., Boiwe, T., Söderberg, B.-O., Tapia, O., Brändén, C.-I., and Åkeson, Å. (1976) *J. Mol. Biol. 102*, 27−59.
6. Eklund, H., Brändén, C.-I., and Jörnvall, H. (1976) *J. Mol. Biol. 102*, 61−73.
7. Park, D.-H., and Plapp, B. V. (1991) *J. Biol. Chem. 266*, 13296−13302.
8. Hubatsch, I., Zeppezauer, M., Waidelich, D., and Bayer, E. (1993) *Adv. Exp. Med. Biol. 328*, 451−455.
9. Brändén, C.-I. (1977) in *Pyridine Nucleotide-Dependent Dehydrogenases* (Sund, H., Ed.) pp 325−338, Walter de Gruyter, Berlin, New York.
10. Park, D.-H., and Plapp, B. V. (1992) *J. Biol. Chem. 267*, 5527−5533.
11. Adolph, H. W., Kiefer, M., and Cedergren-Zeppezauer, E. (1997) *Biochemistry 36*, 8743−8754.
12. Adolph, H. W., Maurer, P., Schneider-Bernlöhr, H., Sartorius, C., and Zeppezauer, M. (1991) *Eur. J. Biochem. 201*, 615−625.
13. Hubatsch, I., Maurer, P., Engel, D., and Adolph, H. W. (1995) *J. Chromatogr. A 711*, 105−112.
14. Adolph, H. W., Kiefer, M., and Zeppezauer, M. (1993) *Adv. Exp. Med. Biol. 328*, 401−410.
15. Viola, R. E., Cook, P. F., and Cleland, W. W. (1979) *Anal. Biochem. 96*, 334−340.
16. Plapp, B. V. (1973) *Arch. Biochem. Biophys. 156*, 112−114.
17. Theorell, H., and Yonetani, T. (1963) *Biochem. Z. 338*, 537−553.
18. Hinsberg, W., and Houle, F. http://www.almaden.ibm.com/st/msim/ckspage.html
19. Teng, T. Y. (1990) *J. Appl. Crystallogr. 23*, 387−391.
20. Otwinowski, Z., and Minor, W. (1997) *Methods Enzymol. 276*, 307−326.
21. Bruenger, A. T. (1992) *Nature 355*, 472−475.
22. Navaza, J. (1994) *Acta Crystallogr. A50*, 157−163.
23. Jones, T. A., Zou, J. Y., Cowan, S. W., and Kjeldgaard, M. (1991) *Acta Crystallogr. A47*, 110−119.
24. Murshudov, G. N., Vagin, A. A., and Dodson, E. J. (1997) *Acta Crystallogr. D53*, 240−255.
25. CCP4 (1994) *Acta Crystallogr. D50*, 760−763.
26. Lamzin, V. S., and Wilson, K. S. (1997) *Methods Enzymol. 277*, 269−305.
27. Vriend, G. (1990) *J. Mol. Graph. 8*, 52−56.
28. Vriend, G., and Sander, C. (1993) *J. Appl. Crystallogr. 26*, 47−60.
29. Theorell, H., and McKinley-McKee, J. S. (1961) *Acta Chem. Scand. 15*, 1811−1833.
30. Bignetti, E., Rossi, G. L., and Zeppezauer, E. (1979) *FEBS Lett. 100*, 17−22.
31. Eklund, H., Samama, J.-P., Wallén, L., Brändén, C. I., Åkeson, Å., and Jones, T. A. (1981) *J. Mol. Biol. 146*, 561−587.
32. Al-Karadaghi, S., Cedergren-Zeppezauer, E., Hövmoller, S., Petratos, K., Terry, H., and Wilson, K. S. (1995) *Acta Crystallogr. D50*, 793−807.
33. Colonna-Cesari, F., Perahia, D., Karplus, M., Eklund, H., Brändén, C.-I., and Tapia, O. (1986) *J. Biol. Chem. 261*, 15273−15280.
34. Eklund, H., Samama, J.-P., and Jones, T. A. (1984) *Biochemistry 23*, 5992−5996.
35. Cedergren-Zeppezauer, E., Samama, J.-P., and Eklund, H. (1982) *Biochemistry 21*, 4895−4908.
36. Cedergren-Zeppezauer, E. S. (1986) in *Zinc Enzymes* (Bertini, I., Luchinat, C., Maret, W., Zeppezauer, M., Eds.) pp 393−415, Birkhäuser, Basel.

37. Ramaswamy, S., Eklund, H., and Plapp, B. V. (1994) *Biochemistry 33*, 5230−5237.
38. Ramaswamy, S., Scholze, M., and Plapp, B. V. (1997) *Biochemistry 36*, 3522−3527.
39. Li, H., Hallows, W. H., Punzi, J. S., Pankiewicz, K. W., Watanabe, K. A., and Goldstein, B. M. (1994) *Biochemistry 33*, 11734−11744.
40. Plapp, B. V., Sogin, D. C., Dworschack, R. T., Bohlken, D. P., and Woenkhaus, C. (1986) *Biochemistry 25*, 5396−5402.
41. Meijers, R. (2000) Ph.D. Thesis, University of Amsterdam, The Netherlands.
42. Dickinson, F. M., and Dalziel, K. (1967) *Biochem. J. 104*, 165−172.
43. Stone, C. L., Li, T.-K., and Bosron, W. F. (1989) *J. Biol. Chem. 264*, 11112−11116.
44. Höög, J. O., Eklund, H., and Jörnvall, H. (1992) *Eur. J. Biochem. 205*, 519−526.
45. Kraulis, P. J. (1991) *J. Appl. Crystallogr. 24*, 946−950.
46. Sayle, R. (1994) *RasMol v2.5: A Molecular Visualisation Program.*

BI001376S